Master integrals contributing to two-loop leading colour QCD helicity amplitudes for top-quark pair production in the gluon fusion channel

Ekta Chaubey⋆

Dipartimento di Fisica and Arnold-Regge Center, Università di Torino, and INFN, Sezione di Torino, Via P. Giuria 1, I-10125 Torino, Italy

⋆ ekta@to.infn.it

15th International Symposium on Radiative Corrections: Applications of Quantum Field Theory to Phenomenology, FSU, Tallahasse, FL, USA, 17-21 May 2021

Abstract

We discuss the analytic structure of the master integrals relevant for computing the complete set of leading-colour analytic helicity amplitudes for top-quark pair production via gluon fusion at two loops in QCD. This includes corrections due to massive fermion loops which give rise to integrals involving elliptic curves. We also elaborate on the structure of singularities that play an important role in the numerical evaluation of the iterated integrals and their analytic continuation.

1 Introduction

The top quark is an important ingredient in understanding the fundamental forces and in particular of the electroweak symmetry breaking mechanism, due to its large mass. The Higgs potential depends on its value and hence a precise understanding of the top quark is imperative.

In the computation of two-loop amplitudes for QCD corrections to top-quark pair production, we start including internal masses a more complicated class of special functions start to appear. These functions include integrals over elliptic curves, which have been an area of interest recently [1–9]. The is also the reason why the only complete two-loop amplitudes for QCD corrections to top-quark pair production were available numerically [10–12] until very recently. A study of a set of helicity amplitudes for top-quark pair production in the leading colour approximation has been recently published in [13]. These helicity amplitudes contained complete information in the narrow width approximation about top quark decays. This included for the first time, the contributions from heavy fermion loops. These contributions

gave rise to iterated integrals involving multiple elliptic curves, which were included in the analytic form of the helicity amplitudes. These amplitudes were obtained by sampling Feynman diagrams with finite field arithmetic [14–19]. Along with this, a numerical evaluation of the final amplitudes in Euclidean, as well as physical region, was studied.

The computation of perturbative contributions at two-loop order with massive internal lines involves a large number of steps, each with some technical bottlenecks. In these proceedings, we elaborate further on the analytic computations of the planar master integrals that were presented in [13] along with discussing the technical bottlenecks in the numerical evaluation with elliptic kernels containing multiple elliptic curves. The master integrals that contribute to these amplitudes also included master integrals from an additional two-loop integral topology. These integrals were not available previous to the publication [13], and also contained two elliptic master integrals. For these additional elliptic integrals we also obtained the (canonical form) differential equation [6, 20–24] and expressed the results in terms of iterated integrals [25].

2 Definitions

We begin by first reviewing the definition of Chen's iterated integrals [26] and an elliptic curve.

2.1 Iterated integrals

Consider a path γ on an n-dimensional manifold M with starting point $x_i = \gamma(0)$ and endpoint $x_f = \gamma(1)$, $\gamma : [0,1] \to M$. Let us also consider a set of differential 1-forms $\{\omega_i\}$ and their pullbacks to the interval $[0,1]$, which we denote by $f_j(\lambda)\, d\lambda = \gamma^* \omega_j$. The k-fold iterated integral over $\omega_1, ..., \omega_k$ along γ is defined as

$$I_\gamma(\omega_1, ..., \omega_k; \lambda) = \int_0^\lambda d\lambda_1 f_1(\lambda_1) \int_0^{\lambda_1} d\lambda_2 f_2(\lambda_2) ... \int_0^{\lambda_{k-1}} d\lambda_k f_k(\lambda_k) \tag{1}$$

$$= \int_0^\lambda d\lambda_1 f_1(\lambda_1) I_\gamma(\omega_2, ..., \omega_k; \lambda_1), \tag{2}$$

where we define the 0-fold integrals as $I_\gamma(; \lambda) = 1$. The iterated integrals defined in Eq. (1) have many useful properties [27]. Some well-known examples of iterated integrals are the multiple polylogarithms (MPLs) [28], which are a special class of functions, where the 1-forms ω_i are such that $\gamma^* \omega_j = \frac{d\lambda}{\lambda - c}$, for some $c \in \mathbb{C}$. The class of MPLs is quite well understood. There exist many tools for their algebraic manipulation and numerical evaluation [29–31]. However, it is not always possible to express all master integrals in terms of these functions. This is especially true in computations that involve massive internal particles, where we often encounter elliptic curves in the analytic structure of the master integrals.

For our work, the most important property is regarding the decomposition of the path γ. Let there be two paths $\alpha, \beta \colon [0,1] \to M$, such that $\beta(0) = \alpha(1)$ and let $\gamma = \alpha\beta$ be the path obtained by concatenating α and β. Then we can decompose

$$I_\gamma(\omega_1, ..., \omega_k; \lambda) = \sum_{i=0}^k I_\beta(\omega_1, ..., \omega_i; \lambda) I_\alpha(\omega_{i+1}, ..., \omega_k; \lambda). \tag{3}$$

2.2 Elliptic curves

A generic quartic form of an elliptic curve E is given by the equation

$$E : w^2 - (z - z_1)(z - z_2)(z - z_3)(z - z_4) = 0, \tag{4}$$

where the $z_i \in \mathbb{C}$. The z_i define the properties of the elliptic curve and are generally functions of the kinematic variables $x = (x_1, ..., x_n)$: $z_j = z_j(x)$, $j \in \{1, 2, 3, 4\}$. An elliptic curve is associated with two elliptic periods ψ_i. In order to define these elliptic periods, let us introduce the auxiliary variables Z_i as

$$Z_1 = (z_2 - z_1)(z_4 - z_3), \quad Z_2 = (z_3 - z_2)(z_4 - z_1), \quad Z_3 = (z_3 - z_1)(z_4 - z_2). \quad (5)$$

The Z_i satisfy the relation $Z_1 + Z_2 = Z_3$, and can be used to define the modulus k^2 and the complementary modulus $\bar{k}^2$ of the elliptic curve E as $k^2 = \frac{Z_1}{Z_3}$, and $\bar{k}^2 = 1 - k^2 = \frac{Z_2}{Z_3}$. Then we can choose the two elliptic periods ψ_i associated to the elliptic curve E as $\psi_1 = \frac{4K(k)}{Z_3^{\frac{1}{2}}}$, and $\psi_2 = \frac{4iK(\bar{k})}{Z_3^{\frac{1}{2}}}$, where K is the complete elliptic integral of the first kind $K(\lambda) = \int_0^1 \frac{dt}{\sqrt{(1-t^2)(1-\lambda t^2)}}$.

3 Analytic form of the master integrals

In this section, let us discuss the analytic structure of the master integrals contributing to our scattering amplitudes. In Fig 1 and Fig 2, we see some examples of integrals needed to compute an analytic form of the finite remainder for the helicity amplitude. All the relevant one- and two-loop master integrals that do not involve a closed top-loop, for example, the first two topologies from Fig. 1, are expressible in terms of MPLs [32,33]. The two-loop topologies that involve a single top-quark closed-loop, for example for the last three topologies from Fig. 1, the master integrals contain elliptic curves [2,3].
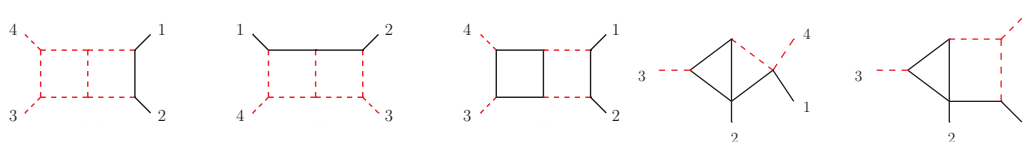
Figure 1: Master integral topologies. Black-solid lines correspond to massive particles, red-dashed lines correspond to massless particles. This figure is from [13] licensed under CC-BY 4.0.

3.1 Elliptic curves in the master integrals

In our work, the dependence of iterated integrals on elliptic curves enters through the appearance of elliptic periods in the integration kernels. The topbox diagram (Fig. 2b) has three elliptic sub-sectors corresponding to three different elliptic curves. These curves can be obtained from the maximal cuts in the Baikov representation [34–36]. We identify the three different elliptic curves by the labels a, b, and c according to the diagrams depicted in Fig. 2.

The sunrise graph (Fig. 2a) is associated with the elliptic curve $E^{(a)}$. The analytic results for this topology can be written in terms of iterated integrals of modular forms, and are well-suited for numerical evaluation [4,8,9,37]. The second elliptic curve $E^{(b)}$ is the one associated with the topbox sector itself (Fig. 2b). The third elliptic curve $E^{(c)}$ comes from yet another elliptic

(a) The sunrise topology

(b) The topbox topology

(c) The bubblebox topology
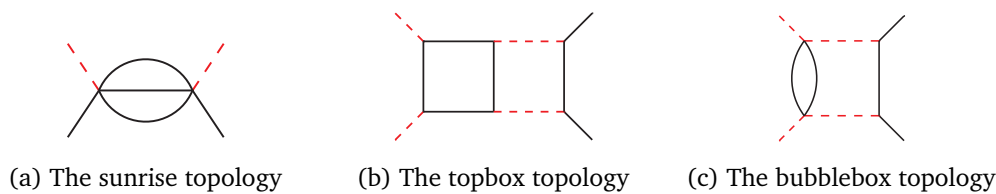
Figure 2: Topologies in the topbox family that are associated with the elliptic curves $E^{(a)}$, $E^{(b)}$ and $E^{(c)}$. Black-solid lines correspond to massive particles, red-dashed lines correspond to massless particles. This figure is from [13] licensed under CC-BY 4.0.

sub-sector, the bubblebox sector (Fig. 2c). All the corresponding quartics (z_i's) are given by

$$
z_1^{(a)} = \frac{t - 4m^2}{\mu^2}, \quad z_2^{(a)} = \frac{-m^2 - 2m\sqrt{t}}{\mu^2}, \quad z_3^{(a)} = \frac{-m^2 + 2m\sqrt{t}}{\mu^2}, \quad z_4^{(a)} = \frac{t}{\mu^2},
$$

$$
z_1^{(b)} = \frac{t - 4m^2}{\mu^2}, \quad z_2^{(b)} = \frac{-m^2 - 2m\sqrt{t + \frac{(m^2 - t)^2}{s}}}{\mu^2}, \quad z_3^{(b)} = \frac{-m^2 + 2m\sqrt{t + \frac{(m^2 - t)^2}{s}}}{\mu^2},
$$

$$
z_4^{(b)} = \frac{t}{\mu^2},
$$

$$
z_1^{(c)} = \frac{t - 4m^2}{\mu^2}, \qquad z_2^{(c)} = \frac{1}{\mu^2}\left(-m^2\frac{(s + 4t)}{(s - 4m^2)} - \frac{2}{4m^2 - s}\sqrt{sm^2\left(st + (m^2 - t)^2\right)}\right),
$$

$$
z_3^{(c)} = \frac{1}{\mu^2}\left(-m^2\frac{(s + 4t)}{(s - 4m^2)} + \frac{2}{4m^2 - s}\sqrt{sm^2\left(st + (m^2 - t)^2\right)}\right), \qquad z_4^{(c)} = \frac{t}{\mu^2}. \tag{6}
$$

3.2 New elliptic master integrals

In addition to the integral topologies discussed above, for which the analytic results were already known, we needed to include contributions from the so-called penta-triangle topology (the last two topologies in Fig. 1). We cast the differential equations of all the master integrals of this topology in a canonical form [6, 24],

$$
d\vec{\mathcal{J}} = \epsilon A\vec{\mathcal{J}}, \quad A = A_x\, dx + A_y\, dy, \tag{7}
$$

where A does not depend on ϵ and is rational in the kinematic variables (x, y). The kinematic variables x and y are defined by

$$
-\frac{s}{m_t^2} = \frac{(1 - x)^2}{x}, \qquad \frac{t}{m_t^2} = y. \tag{8}
$$

These new master integrals can be now computed order by order in ϵ from the differential equation given in Eq. (7). We integrated the differential equation from a base point $(x_0, y_0) = (0, 1)$ (corresponding to $s = \infty$ and $t = m^2$) and expressed the results of the master integrals iteratively in the expansion parameter ϵ. The boundary values of the integrals at different orders in ϵ were obtained from the regularity of the differential system at the point $x, y = (1, 1)$, where these two master integrals vanish.

Let us discuss the analytic structure of these master integrals. Both of these integrals receive contributions from the elliptic topbox sub-sectors and hence contain elliptic iterated integrals themselves. The fourth integral from Fig. 1 has a sunrise in its sub-sectors and hence is associated with the elliptic curve a. The fifth integral from Fig. 1, on the other hand, contains an elliptic subsector from the topbox which is associated with the elliptic curve b [3] and hence is also itself elliptic.

4 Numerical evaluations of elliptic iterated integrals

The analytic form of the amplitude is expressed using the iterated integrals, which contain transcendental functions, inside the one forms, in the form of elliptic periods and their derivatives. Since there are three different elliptic curves, the numerical evaluation of these objects becomes highly non-trivial. In this section, we discuss the numerical computation of all the master integrals. The integrals expressible in terms of MPLs can be evaluated to high precision, for example, using GINAC [38]. For the elliptic master integrals, we use the fact iterated integrals satisfy the path decomposition formula. We basically need to integrate these integrals from the base point $(x = 0, y = 1)$ to any x and y. For this, we use a path involving multiple line segments and use the path decomposition formula to patch together the contribution over all the segments. Choosing the path segments can be often tricky since we need to take into consideration both spurious as well as physical singularities of the system. We may often need multiple path segments to get a better convergence of the results. We now go through the techniques of the numerical evaluation of these iterated integrals in Euclidean and the physical regions one by one.

In the Euclidean region the iterated integrals are real. To compute the iterated integrals in this region, we start from a small neighborhood of the boundary point. This makes our task relatively straightforward. We split the integration path from the boundary point $(0, 1)$ to any point (x, y) and integrate over each of these segments, where we series expand the kernels around some points along the paths. Using the path decomposition formula Eq. (3), we then patch together the contribution to obtain the final result. For example, we may choose the following path segments: α, from $(0, 0)$ to $(x, 0)$ and β, from $(x, 0)$ to (x, y). Over the first segment, all the master integrals in our case compute to only MPLs, which we can evaluate to very high precision, as mentioned before. To integrate along the second segment, we may expand all integration kernels around $y = 1$. If we wish to integrate to a point y not close to 1, we may use more segments along y and use the path decomposition formula recursively.

Let us now discuss how the computations change for the physical region. For our case, the physical region is governed by the following equations ($m_t^2 = 1$):

$$ s \geq 4, \qquad G(p_1, p_2, p_3) \geq 0 \implies s(-t^2 - st + 2t - 1) \geq 0, $$

where G is the Gram-determinant, see point P in Fig. 3. To go from the Euclidean to the physical region, we analytically continue the iterated integrals around the physical branch points and across the branch cuts appropriately. As also explained before, we do series expansion of the integrands and use multiple one-dimensional path segments to reach our final point in the physical region. The choice of the path is again governed by the radius of convergence of the series. This in turn depends on the singularities present in the kernels. In the next section, we look at the singularity structure of our system of differential equations. Since here we are using many path segments, it is important to properly choose the number of path segments and their sizes. This is important because the number of segments affects the speed of computation of our iterated integrals. In addition, it is needed to make sure that the series solution converges properly on each of these segments. Let us briefly discuss the performance of individual type of elliptic iterated integrals. The analytic continuation of integrals having only one parameter dependence is relatively easier and has also been heavily discussed in the literature [7, 9, 37]. The analytic continuation of all the iterated integrals that contained multiple elliptic curves, however, is much more involved. At the boundary of the region, we choose a proper $i\epsilon$ prescription to analytically continue these kernels.

We now look at the singularity structure of our differential system, which plays a crucial role in the numerical evaluation of the master integrals.
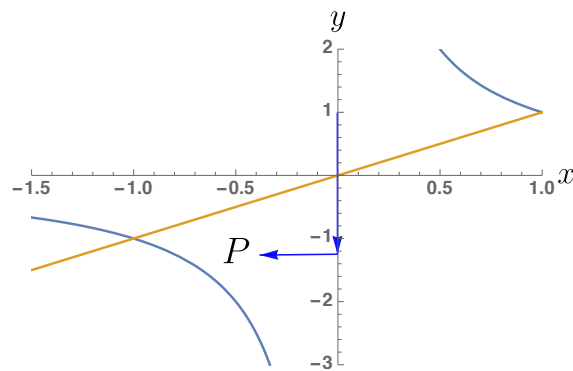
Figure 3: Integrating to a point P in the physical region. This figure is from [13] licensed under CC-BY 4.0.

4.1 Choice of path

The choice of path is even more important to evaluate the master integrals written in terms of iterated integrals, in the physical region. Below we explain the observations that motivate our choice for the path.

4.1.1 Technical challenges

Let us start by integrating the iterated integrals in our system first along x ($y = constant$) and then along y ($x = constant$), also for the physical region, as we do for the Euclidean region. We immediately hit a problem. On the line x=y, we encounter some functions which are not elementary. A general form of the integrals arising in this case has the form

$$\int \frac{t^m \log(-\log(t))}{\log(t)^n} dt, \int \frac{t^m Ei(m\log(t))}{\log(t)} dt, \int \frac{t^4 \, \text{LogIntegral}(t)}{\log(t)^n} dt, \tag{9}$$

where Ei is the Exponential Integral. There is no power series expansion (specifically around the point of expansions), but only an asymptotic series expansion [39], of LogIntegral(x) or $Ei(\log(x)n)$, for any integer n. The occurrence of such functions can be understood as follows. Many of our kernels contain periods in the denominator, which give rise to logarithms when series expanded. These logarithms give rise to the functions above upon integration. It is worth noting that these kernels cannot be handled in this form by any program which performs a generalized series expansion of the kernels, for example [40], as we will face the same problems. If we change our order of integration such that we first integrate along y and then along x, we circumvent these problems. All the kernels giving rise to the type of functions mentioned above drop out, or become simpler, because of the boundary conditions. In addition, while crossing the line $y = 0$, we get a singularity for all the kernels having periods belonging to the sunrise topology. Whereas for the elliptic kernels having both x and y dependence, there is a singularity on the line $x = y$, which is the line crossing over to the physical region. Both these types of singularities coincide, for the path shown in Fig. 3 at the point (0,0). Therefore it is easier to integrate all the iterated integrals first along y and then along x, motivating our choice of paths.

4.1.2 Singularity structure of the differential system

On the path shown in Fig. 3, after integrating along $x = 0$, we need to integrate along $y = constant$ line. On this second line, it is again important to choose the point of expansion

and the number of path segments carefully. For the second line, the singularities of the kernels in x change depending on the value of y. A good rule of thumb is that the segments should not be larger than half the radius of convergence of the series expansion [5]. Below we show all the singularities, computed naively by considering zeroes of all the denominators, of the iterated integrals at particular values of y. For comparisons, we show the singularity structure for two values of y, $y = 0.2$ and -1.75, before and after crossing over to the physical region. It is clear from the pictures that for the point y=-1.75 (also true for other points in this region), the radius of convergence is relatively big. This lets us choose fewer segments on this path, eventually making the integration time faster.

(a) Singularities in the x plane for y=0.2   (b) Singularities in the x plane for y=-1.75
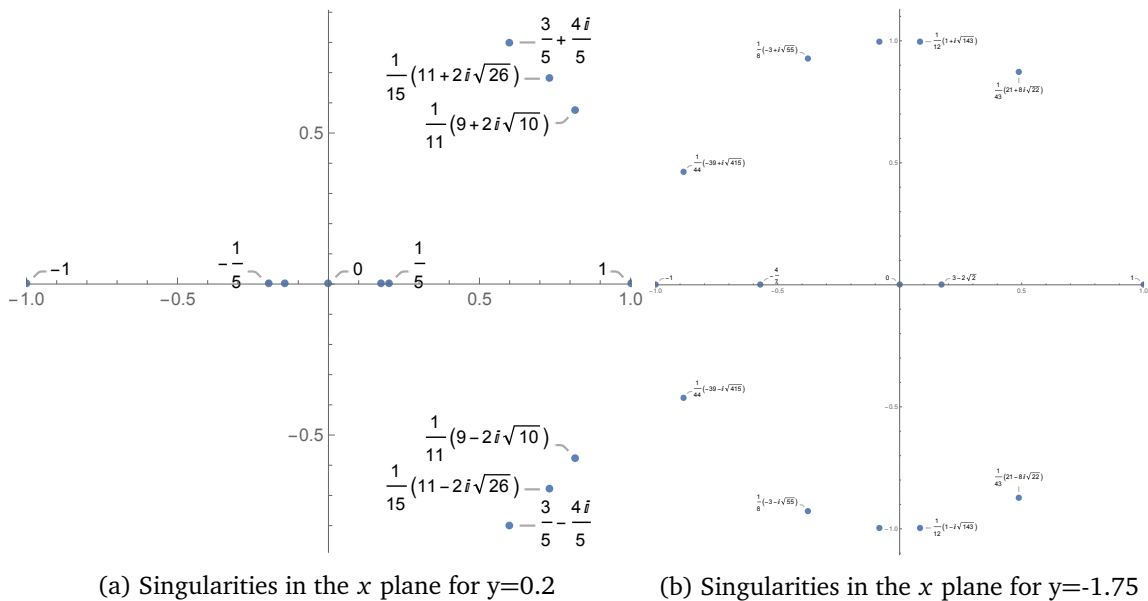
Figure 4: Singularities of the differential system of topbox.

The downside of choosing a path like in Fig. 3 is that the kernels no longer simplify to MPLs on either of the parts, $x = constant$ or $y = constant$, as was the case for the path chosen for the Euclidean region. Using the path decomposition formula also in this case, we can patch together the contributions from the different segments and compute the iterated integrals over the whole path. For the integrals belonging to the topbox family, we analytically continue all the iterated integrals associated with the curves a and b to the physical region, along with all the integrals depending only on MPLs.

Analogously we can integrate into other phase-space regions. Another approach to perform the integration in different phase space regions is to start integrating from a point already in that region. The upside of this is that we do not need to analytically continue across the branch cut. The downside is that for this we need to compute the boundary conditions at new base points.

5   Conclusion

In these proceedings, we discussed the master integrals needed to compute a complete set of analytic helicity amplitudes for the planar corrections to top quark pair production via gluon fusion at two-loop order in QCD. We explained the analytic form of the master integrals, looked at the singularity structure of the system of differential equations of these master integrals, and studied their numerical evaluation. These integrals give rise to a set of special functions which

are associated with three elliptic curves. As we elaborated in this article, the numerical evaluation of iterated integrals with these kernels is complicated in the current form. Here we further discussed some of the challenges faced. Nevertheless, it was the first time that amplitude level expressions were obtained for the planar corrections to top quark pair production including the top quark loops, which resulted in analytic expressions involving elliptic curves in the finite remainder. Despite the growth in analytic complexity, this study of the numerical evaluation is one of the few such studies which includes functions with multiple elliptic curves for phenomenological applications. In addition, we find interesting insights manifesting in the form of relations between elliptic iterated integrals that leads to analytic simplification and complete cancellation of the universal IR and UV poles.

Acknowledgements

This project has received funding from the European Union's Horizon 2020 research and innovation programmes *New level of theoretical precision for LHC Run 2 and beyond* (grant agreement No 683211) and *High precision multi-jet dynamics at the LHC* (grant agreement No 772009).

References

[1] L. Adams, E. Chaubey and S. Weinzierl, *Simplifying Differential Equations for Multiscale Feynman Integrals beyond Multiple Polylogarithms*, Phys. Rev. Lett. **118**, 141602 (2017), doi:10.1103/physrevlett.118.141602.

[2] L. Adams, E. Chaubey and S. Weinzierl, *Planar Double Box Integral for Top Pair Production with a Closed Top Loop to all orders in the Dimensional Regularization Parameter*, Phys. Rev. Lett. **121**, 142001 (2018), doi:10.1103/PhysRevLett.121.142001.

[3] L. Adams, E. Chaubey and S. Weinzierl, *Analytic results for the planar double box integral relevant to top-pair production with a closed top loop*, J. High Energy Phys. **10**, 206 (2018), doi:10.1007/JHEP10(2018)206.

[4] L. Adams and S. Weinzierl, *Feynman integrals and iterated integrals of modular forms*, arXiv:1704.08895.

[5] S. Abreu, H. Ita, F. Moriello, B. Page, W. Tschernow and M. Zeng, *Two-loop integrals for planar five-point one-mass processes*, J. High Energy Phys. **None**, 117 (2020), doi:10.1007/jhep11(2020)117.

[6] L. Adams and S. Weinzierl, *The ε-form of the differential equations for Feynman integrals in the elliptic case*, Phys. Lett. B **781**, 270 (2018), doi:10.1016/j.physletb.2018.04.002.

[7] C. Bogner, A. Schweitzer and S. Weinzierl, *Analytic continuation and numerical evaluation of the kite integral and the equal mass sunrise integral*, Nucl. Phys. B **922**, 528 (2017), doi:10.1016/j.nuclphysb.2017.07.008.

[8] J. Broedel, C. Duhr, F. Dulat, R. Marzucca, B. Penante and L. Tancredi, *An analytic solution for the equal-mass banana graph*, J. High Energy Phys. **09**, 112 (2019), doi:10.1007/JHEP09(2019)112.

[9] S. Abreu, M. Becchetti, C. Duhr and R. Marzucca, *Three-loop contributions to the ρ parameter and iterated integrals of modular forms*, J. High Energy Phys. **02**, 050 (2020), doi:10.1007/JHEP02(2020)050.

[10] M. Czakon, *Tops from light quarks: Full mass dependence at two-loops in QCD*, Phys. Lett. B **664**, 307 (2008), doi:10.1016/j.physletb.2008.05.028.

[11] P. Bärnreuther, M. Czakon and P. Fiedler, *Virtual amplitudes and threshold behaviour of hadronic top-quark pair-production cross sections*, J. High Energy Phys. **02**, 078 (2014), doi:10.1007/JHEP02(2014)078.

[12] L. Chen, M. Czakon and R. Poncelet, *Polarized double-virtual amplitudes for heavy-quark pair production*, J. High Energy Phys. **03**, 085 (2018), doi:10.1007/JHEP03(2018)085.

[13] S. Badger, E. Chaubey, H. Bayu Hartanto and R. Marzucca, *Two-loop leading colour QCD helicity amplitudes for top quark pair production in the gluon fusion channel*, J. High Energy Phys. **06**, 163 (2021), doi:10.1007/JHEP06(2021)163.

[14] P. S. Wang, *A p-adic algorithm for univariate partial fractions*, In Proceedings of the Fourth ACM Symposium on Symbolic and Algebraic Computation, SYMSAC '81, pp. 212–217. ACM, New York, NY, USA, ISBN 0-89791-047-8, doi:10.1145/800206.806398 (1981).

[15] P. S. Wang, M. J. T. Guy and J. H. Davenport, *P-adic reconstruction of rational numbers*, SIGSAM Bull. **16**, 2 (1982), doi:10.1145/1089292.1089293.

[16] B. Trager, *ISSAC '06: Proceedings of the 2006 International Symposium on Symbolic and Algebraic Computation*. ACM, New York, NY, USA, ISBN 1-59593-276-3, 505060 (2006).

[17] A. von Manteuffel and R. M. Schabinger, *A novel approach to integration by parts reduction*, Phys. Lett. B **744**, 101 (2015), doi:10.1016/j.physletb.2015.03.029.

[18] T. Peraro, *Scattering amplitudes over finite fields and multivariate functional reconstruction*, J. High Energy Phys. **12**, 030 (2016), doi:10.1007/JHEP12(2016)030.

[19] T. Peraro, *FiniteFlow: multivariate functional reconstruction using finite fields and dataflow graphs*, J. High Energy Phys. **07**, 031 (2019), doi:10.1007/JHEP07(2019)031.

[20] Z. Bern, L. Dixon and D. A. Kosower, *Dimensionally-regulated pentagon integrals*, Nucl. Phys. B **412**, 751 (1994), doi:10.1016/0550-3213(94)90398-0.

[21] A. V. Kotikov, *Differential equations method. New technique for massive Feynman diagram calculation*, Phys. Lett. B **254**, 158 (1991), doi:10.1016/0370-2693(91)90413-K.

[22] E. Remiddi, *Differential equations for Feynman graph amplitudes*, Nuovo Cim. A **110**, 1435 (1997), doi:10.1007/BF03185566.

[23] T. Gehrmann and E. Remiddi, *Differential equations for two-loop four-point functions*, Nucl. Phys. B **580**, 485 (2000), doi:10.1016/S0550-3213(00)00223-6.

[24] J. M. Henn, *Multiloop Integrals in Dimensional Regularization Made Simple*, Phys. Rev. Lett. **110**, 251601 (2013), doi:10.1103/PhysRevLett.110.251601.

[25] J. Ablinger, J. Blümlein, A. De Freitas, M. van Hoeij, E. Imamoglu, C. G. Raab, C.-S. Radu and C. Schneider, *Iterated elliptic and hypergeometric integrals for Feynman diagrams*, J. Math. Phys. **59**, 062305 (2018), doi:10.1063/1.4986417.

[26] K.-T. Chen, *Iterated path integrals*, Bull. Amer. Math. Soc. **83**, 831 (1977), doi:10.1090/S0002-9904-1977-14320-6.

[27] F. Brown, *Iterated integrals in quantum field theory*, in Geometric and Topological Methods for Quantum Field Theory, Cambridge University Press, Cambridge (2011), doi:10.1017/CBO9781139208642.006.

[28] A. B. Goncharov, *Multiple polylogarithms, cyclotomy and modular complexes*, arXiv:1105.2076.

[29] C. Duhr and F. Dulat, *PolyLogTools — polylogs for the masses*, J. High Energy Phys. **08**, 135 (2019), doi:10.1007/JHEP08(2019)135.

[30] E. Panzer, *Feynman integrals and hyperlogarithms*, Ph.D. thesis, Humboldt U., doi:10.18452/17157 (2015).

[31] C. Bauer, A. Frink and R. Kreckel, *Introduction to the GiNaC Framework for Symbolic Computation within the C++ Programming Language*, J. Symb. Comput. **33**, 1 (2002), doi:10.1006/jsco.2001.0494.

[32] S. Moch, P. Uwer and S. Weinzierl, *Nested sums, expansion of transcendental functions, and multiscale multiloop integrals*, J. Math. Phys. **43**, 3363 (2002), doi:10.1063/1.1471366.

[33] J. Borwein, D. Bradley, D. Broadhurst and P. Lisoněk, *Special values of multiple polylogarithms*, Trans. Amer. Math. Soc. **353**, 907 (2000), doi:10.1090/S0002-9947-00-02616-7.

[34] H. Frellesvig and C. G. Papadopoulos, *Cuts of Feynman Integrals in Baikov representation*, J. High Energy Phys. **04**, 083 (2017), doi:10.1007/jhep04(2017)083.

[35] A. Primo and L. Tancredi, *On the maximal cut of Feynman integrals and the solution of their differential equations*, Nucl. Phys. B **916**, 94 (2017), doi:10.1016/j.nuclphysb.2016.12.021.

[36] A. Primo and L. Tancredi, *Maximal cuts and differential equations for Feynman integrals. An application to the three-loop massive banana graph*, Nucl. Phys. B **921**, 316 (2017), doi:10.1016/j.nuclphysb.2017.05.018.

[37] C. Duhr and L. Tancredi, *Algorithms and tools for iterated Eisenstein integrals*, J. High Energy Phys. **02**, 105 (2020), doi:10.1007/JHEP02(2020)105.

[38] J. Vollinga and S. Weinzierl, *Numerical evaluation of multiple polylogarithms*, Comput. Phys. Commun. **167**, 177 (2005), doi:10.1016/j.cpc.2004.12.009.

[39] M. Abramowitz and I. Stefun, *Handbook of Mathematical Functions with Formulas, Graphs, and Mathematical Tables*, Dover, ISBN 978-0-486-61272-0 (1964).

[40] M. Hidding, *DiffExp, a Mathematica package for computing Feynman integrals in terms of one-dimensional series expansions*, Comput. Phys. Commun. **269**, 108125 (2021), doi:10.1016/j.cpc.2021.108125.